What controls the temperature of the Arctic stratosphere during the spring?

Paul A. Newman

NASA Goddard Space Flight Center, Greenbelt, MD

Eric R. Nash

Emergent Information Technologies, Inc., Vienna, VA

Joan E. Rosenfield

SAIC/General Sciences Corporation, Beltsville, MD

Short title: TEMPERATURE OF THE SPRING ARCTIC STRATOSPHERE

Abstract.

Understanding the mechanisms that control the temperature of the polar lower stratosphere during spring is key to understanding ozone loss in the Arctic polar vortex. Spring ozone loss rates are directly tied to polar stratospheric temperatures by the formation of polar stratospheric clouds, and the conversion of chlorine species to reactive forms on these cloud particle surfaces. In this paper, we study those factors that control temperatures in the polar lower stratosphere. We use NCEP/NCAR reanalysis data covering the last two decades to investigate how planetary wave driving of the stratosphere is connected to polar temperatures. In particular, we show that planetary waves forced in the troposphere in mid- to late winter (January–February) are principally responsible for the mean polar temperature during the March period. These planetary waves are forced by both thermal and orographic processes in the troposphere, and propagate into the stratosphere in the mid and high latitudes. Strong mid-winter planetary wave forcing leads to a warmer Arctic lower stratosphere in early spring, while weak mid-winter forcing leads to cooler Arctic temperatures.

1. Introduction

1.1. Background

The temperature of the polar lower stratosphere is mainly controlled by the variation of the solar declination from the winter to spring solstices, and by the distribution of radiatively active trace gases such as ozone, water, and carbon dioxide [*Shine,* 1987]. However, during the winter, the Arctic lower stratosphere is considerably warmer than would be expected from a pure radiative calculation [*Fels,* 1982]. This temperature difference is due to waves which propagate up from the troposphere into the stratosphere, where they dissipate. This wave dissipation causes a poleward and downward circulation which acts to warm the polar region and drive it away from the radiative equilibrium [*Andrews et al.,* 1987]. In addition, these waves critically impact concentrations of ozone in the stratosphere.

Brewer [1949] and *Dobson* [1956] first illustrated the long-term slow-rising circulation in the tropics and the slow descent in the extratropics. Simple thermodynamics shows that the polar descent via the Brewer-Dobson circulation acts to warm the polar regions. Numerous two- and three-dimensional modeling studies have shown how this circulation carries ozone from the photochemical production region in the tropical upper stratosphere to the polar lower stratosphere, resulting in the steady accumulation of ozone in the Northern Hemisphere polar lower stratosphere [e.g., *Chipperfield and Jones,* 1999].

Early investigators saw large increases of total ozone and temperature following

major stratospheric warmings [e.g., *London*, 1963]. Our theoretical understanding of the relationship of waves to the stratospheric mass circulation and temperature caught up with observations when it was recognized that the transport circulation [*Plumb*, 1979] was approximated by the residual circulation [*Dunkerton*, 1978]. The relationship of the stratospheric circulations to the wave driving from the troposphere was solidified by *Haynes et al.* [1991] with the development of the "downward control" principle, which simply states that the circulation across an isentropic surface is controlled by upward Rossby and gravity wave propagation which break at higher levels. *Fusco and Salby* [1999] have used this concept to show that the interannual variation of northern hemisphere midlatitude total ozone is coherent with upwelling planetary wave activity.

The discovery of the Antarctic ozone hole by *Farman et al.* [1985] and the recognition of heterogeneous chemical processes as a principal cause of this ozone loss highlighted the important role of polar temperatures. Low temperatures (< 195 K) result in the formation of polar stratospheric clouds (PSCs), which lead to a release of chlorine from reservoir species into reactive forms. The rising of the sun in the polar spring period combined with these low temperatures results in large ozone losses via the ClO-ClO and BrO-ClO catalytic cycles [*Anderson et al.*, 1989].

Since the Arctic winter stratosphere is much warmer than the Antarctic winter stratosphere, PSCs are much less prevalent in the Arctic [*Poole and Pitts*, 1994]. This results in smaller Arctic ozone losses than over Antarctica. However, during the mid-1990s, spring Arctic ozone levels have been extremely low [*Newman et al.*, 1997; *Fioletov et al.*, 1997] and are due to both transport and chemical effects

[*Chipperfield and Jones*, 1999]. *Coy et al.* [1997] showed that the extremely low ozone values of 1997 were accompanied by very low temperatures and extremely weak planetary wave driving of the stratosphere. *Zurek et al.* [1996] have shown that the mid-1990s (Upper Atmosphere Research Satellite period) is characterized by reductions in the frequency of stratospheric warmings. *Pawson and Naujokat* [1997, 1999] have shown that there has been an increase in the areal extent of these low temperatures, especially in late winter. *Waugh et al.*, [1999] showed that the Arctic vortex had much later breakup dates in the 1990s as compared with earlier decades. These studies suggest that the 1990s were characterized by a climatic period of weaker planetary wave driving and lower temperatures.

In this paper we will tighten the connection between the polar lower stratospheric spring temperature in early March and the winter planetary wave driving. We will derive a simple theoretical relationship between the wave driving and the temperature, discuss the data used, and will demonstrate the quantitative relationship between the wave driving and the temperature. We will present the correlation of a variety of parameters to show the full impact of planetary wave driving of the stratosphere.

2. Theoretical formulation

The wave driving of the stratosphere is necessary for understanding the evolution of the stratospheric temperatures, circulation, and the transport of trace gases such as ozone. The transformed Eulerian mean (TEM) circulation provides a wave-mean flow theoretical framework for the overall dynamics of the stratosphere (see *Andrews*

et al. [1987] for a basic description of the TEM). This TEM formulation can be used to directly connect wave effects with the circulation and the temperature of the polar lower stratosphere.

The zonal-mean thermodynamic equation can be simply expressed in the TEM formulation as

$$\frac{\partial \overline{T}}{\partial t} + \overline{w}^* S = \overline{Q}, \tag{1}$$

where $\overline{w}^*$ is the vertical component of the residual circulation, T is the temperature, Q is the heating, t is time, the overbar refers to a zonal-mean quantity, and S is the static stability ($= \partial T/\partial z + g/c_p$, where z is the pressure altitude, g is the gravitational constant, and c_p is the specifi heat at constant pressure).

The vertical residual circulation component is expressed in Eulerian terms as

$$\overline{w}^* = \overline{w} + \frac{1}{a\cos\phi}\,\frac{\partial}{\partial\phi}\left(\frac{\cos\phi\;\overline{v'T'}}{S}\right). \tag{2}$$

where w is the vertical component of the wind, a is the Earth's radius, ϕ is latitude, and the prime indicates departures from the zonal mean. The meridional heat flux is given by $\overline{v'T'}$. In this formulation of $\overline{w}^*$, we have neglected the vertical heat flux ($\overline{w'T'}$), since it is typically quite small in the stratosphere, although it can be quite important for the mesosphere via the heat flux associated with gravity waves.

We approximate the heating as $\overline{Q} = -\alpha(\overline{T} - \overline{T}_{re})$, a standard Newtonian cooling approximation [*Fels.* 1982], where $\overline{T}_{re}$ is the radiative equilibrium temperature and α is the damping rate. *Newman and Rosenfield* [1997] used temperature observations and a diabatic heating model to show that this linear relationship is extremely robust, and

that α^{-1} is approximately 30 days in the lower stratosphere. Because the radiative equilibrium varies slowly with time, the steady-state ($\partial\overline{T}/\partial t = 0$) solution of (1) yields

$$\overline{T}_s = \overline{T}_{re} - \frac{\overline{w}_s^* S}{\alpha}. \tag{3}$$

where the subscript s denotes the steady-state solution value. This steady-state solution shows that the temperature of the lower stratosphere is controlled by the radiative equilibrium temperature and the strength of the residual circulation. A stronger downward circulation produces warmer temperatures, while a weaker circulation leads to colder temperatures closer to the radiative equilibrium. Further, weak thermal damping amplifies the effect of the circulation. While this steady-state solution allows us to examine the year-to-year variation of winter temperatures, it does not shed much light on those factors that impact the polar lower stratospheric temperature during the chemically critical period of late winter.

We can temporally integrate (1) to gain insight into the time-dependent solution. We assume that both the radiative equilibrium temperature and the radiative damping rate are both constant over the periods that we are considering (mid-winter), as will be shown in section 5. We integrate (1) from a time prior to our period of interest ($-t$, early winter, for example) to the day of interest ($t = 0$, approximately early March).

$$\overline{T}(0) = \overline{T}_{re} + e^{-\alpha t}[\overline{T}(-t) - \overline{T}_{re}] - \int_{-t}^{0} e^{\alpha \hat{t}} \overline{w}^* S d\hat{t}. \tag{4}$$

The first term on the right hand side represents the radiative equilibrium temperature. The second term on the right hand side represents the initial deviation from the radiative temperature. This initial temperature deviation is exponentially damped with time.

For a typical damping time scale of 30 days, a temperature deviation will be reduced to 13% of it's value within two months. Hence, early March temperatures would be only weakly dependent on December temperatures. The third term is the weighted integral of the vertical residual circulation. A strong $\overline{w}^*$ occuring in the November-December period will also have limited direct impact on the March polar temperature due to the damping effect. A strong warming in mid-February should have a large impact on early March temperatures.

The steady-state solution to (1) is retrieved from (4) for constant $\overline{w}^*$ and $\alpha t >> 1$. However, the interannual variability of both March polar temperatures and $\overline{w}^*$, combined with the relatively short damping times ($\alpha^{-1} \approx 30$ days), suggests that the steady-state assumption (3) is not valid. Hence, we must use the time-dependent solution (4) for interpreting these temperatures.

Understanding how $\overline{w}^*$ is controlled by planetary waves is the key to connecting the wave driving to polar temperatures. *Haynes et al.* [1991] originally showed how the extratropical diabatic mass flow across a given isentropic surface may be regarded as being controlled exclusively by the Eliassen-Palm (E-P) flux divergence ($\nabla \cdot \mathbf{F}$) distribution above that surface under steady-state conditions. Further, *Haynes et al.* [1991] also show that the downward control principle is generally applicable for longer period, larger scale waves in a time-dependent solution. Hence, the dissipation of vertically propagating planetary waves is a principal forcing of the residual circulation in the polar lower stratosphere.

This control of the residual circulation is mathematically shown via the steady-state

zonal-mean momentum equation in the TEM formulation. Following *Haynes et al.* [1991],

$$\overline{w}^* = -\frac{1}{a\rho_0 \cos\phi}\,\frac{\partial}{\partial\phi}\left[\int_z^\infty \left(\frac{\nabla\cdot\mathbf{F}}{af}\right) d\hat{z}\right], \tag{5}$$

where f is the Coriolis parameter, ρ_0 is the density ($\equiv \rho_s e^{-z/H}$, where H is a mean scale height and ρ_s is the density at 1000 hPa), the E-P flux vector ($\mathbf{F}$) has components $a\rho_0\cos\phi\ (-\overline{u'v'},\ f\,\overline{v'T'}/S)$, and

$$\begin{aligned}\nabla\cdot\mathbf{F} &= -\frac{1}{\cos\phi}\,\frac{\partial}{\partial\phi}(\rho_0\cos^2\phi\ \overline{u'v'}) \\ &\quad + af\cos\phi\,\frac{\partial}{\partial z}\left(\frac{\rho_0\overline{v'T'}}{S}\right).\end{aligned} \tag{6}$$

Integration of (5) from a midlatitude reference latitude ϕ_r to the pole yields the polar cap area-weighted average of $\overline{w}^*$ as

$$\langle\overline{w}^*\rangle_{\phi_r} = \frac{1}{a\rho_0(1-\sin\phi_r)}\int_z^\infty \left\{\frac{\nabla\cdot\mathbf{F}}{af}\right\}_{\phi_r} d\hat{z}, \tag{7}$$

where $\langle\rangle_{\phi_r}$ is the average of the quantity in angle brackets between ϕ_r and the pole (a polar cap area-weighted average, not the global average) and $\{\}_{\phi_r}$ is the quantity in brackets evaluated at ϕ_r. Substituting 6 into 7, choosing a ϕ_r where the first term is small (approximately near 65°N), and integrating we get

$$\langle\overline{w}^*\rangle_{\phi_r} = -\frac{\cos\phi_r}{a(1-\sin\phi_r)}\left\{\frac{\overline{v'T'}}{S}\right\}_{\phi_r}. \tag{8}$$

This equation shows that $\overline{w}^*$ should be anticorrelated with the heat flux. Substituting (8) into (4), we get

$$\begin{aligned}\langle\overline{T}(0)\rangle_{\phi_r} &= \langle\overline{T}_{re}\rangle_{\phi_r} + e^{-\alpha t}[\langle\overline{T}(-t)\rangle_{\phi_r} - \langle\overline{T}_{re}\rangle_{\phi_r}] \\ &\quad + \frac{\cos\phi_r}{a(1-\sin\phi_r)}\int_{-t}^{0} e^{\alpha\hat{t}}\ \{\overline{v'T'}\}_{\phi_r} d\hat{t}.\end{aligned} \tag{9}$$

Therefore, the polar mean temperature is directly correlated with the exponentially weighted integral of the heat flux during the period that precedes the time of interest.

Another important aspect of the eddy heat flux is that it is proportional to the vertical group velocity of a planetary wave [*Edmon et al.*, 1980]. The heat flux for a particular wave is proportional to the square of the wave amplitude, and the vertical and zonal wavenumbers. Since the heat flux is almost always positive [*Newman and Nash,* 2000], the wave energy is always propagating vertically from the troposphere to the stratosphere. Hence, we interchangeably refer to the heat flux as the wave driving of the stratosphere.

The TEM formulation of the thermodynamic equation has been used to show the connection between the circulation and the temperature of the lower stratosphere. We find that the steady-state assumption for the lower stratospheric temperature is generally not valid for the early March period because of the dependence of these March polar temperatures on the highly variable January–February residual circulation. We also find that it is both the direct effect of the diabatic heating, and the weighted impact of the residual circulation that controls the polar lower stratospheric temperature. Further, the temperature anomaly is related to the timing and strength of the residual circulation, and the wave driving of the stratosphere controls the strength of the residual circulation. We find that the heat flux (vertical component of the wave driving) is anticorrelated with the polar vertical residual circulation.

Because of the sensitivity of ozone photochemistry to the temperature during March, we have chosen to focus on the northern hemisphere winter period for understanding

how the dynamics impacts the temperatures during March. Based on the radiative damping time scale (30 days) we estimate that the period from mid-January to late February is critical to understanding March lower stratospheric temperatures.

3. Data sources

We use two meteorological analyses in this paper. These are the National Centers for Environmental Prediction's (NCEP) Climate Prediction Center (CPC) stratospheric analysis and the jointly produced NCEP/NCAR reanalysis. The NCEP/CPC analysis is an operational product which is subject to data changes. In contrast, the NCEP/NCAR reanalysis is a continuous, consistent assimilation system with analyses extending back to 1958. Herein, we use data beginning in 1979 because of the problems associated with analyses prior to incorporation of satellite data [*Pawson and Fiorino*, 1998; *Santer et al.*, 1999].

The NCEP/NCAR reanalyses use the NCEP spectral model with a T62 triangular truncation and satellite temperature retrievals. This analysis system is consistently run for all of the years, such that changes in the archived meteorological fields are either due to changes in observational systems or due to real geophysical processes [*Kalnay et al.*, 1996]. The data are available on pressure levels from 1000 to 10 hPa, and a 2.5° longitude by 2.5° latitude horizontal grid.

The NCEP/CPC produces analyses based on the NCEP T126 GDAS model and use an objective analysis of satellite and radiosonde data to extend the pressure levels from 70 to 0.4 hPa [*Gelman et al.*, 1986; *Nagatani et al.*, 1988; *Finger et al.*, 1993]. The

horizontal grid is a 65 × 65 point stereographic projection which we interpolate to a grid of 5° longitude by 2° latitude. At 100 hPa and below, these data are solely based on the T126 GDAS product. Temperatures and geopotential heights are basic products of this tropospheric-stratospheric hybrid system, while we produce consistent balanced winds at all levels using the method described in *Randel* [1987] and *Newman et al.* [1988].

Newman and Nash [2000] showed that there are 30% peak-to-peak differences between eddy heat fluxes derived from the variety of analyses produced by the various meteorological centers. These differences occurred during the disturbed conditions of the northern hemisphere winter. The large differences result from the differences in stationary planetary waves in the temperature and meridional wind fields. In contrast, planetary-scale transient waves showed excellent agreement amongst the five analyzed data sets used in *Newman and Nash* [2000], and this transient heat flux appears to have a long-term downward trend.

4. The Eddy Heat Flux-Polar Temperature Connection

Using the theoretical considerations of Section 2, the polar lower stratospheric temperature ought to respond to the time-integrated effects of the heat flux. We calculate the wave energy propagating into the stratosphere, represented by $\overline{v'T'}$ in the third term of (9), by averaging the NCEP/NCAR reanalysis total heat flux at 100 hPa between 45°N and 75°N. The time scale of the integration in this term is 20–40 days, as determined by the thermal damping rate (α^{-1}) of *Newman and Rosenfield* [1997]. As a simple test, Figure 1a shows this total heat flux over the period January 15 to February

Figure 1

28 versus the March 1–15 zonal-mean temperature at 50 hPa between 60°N and 90°N, for each year from 1979 to 2000. The figure shows a very strong correlation ($r = 0.82$) between the March temperature and this late winter heat flux. The correlation between temperature and heat flux for the simultaneous period (Figure 1b) is much poorer ($r = 0.25$). The value of 0.82 means that we can account for 15.3 K of the 18.6 K peak-to-peak interannual variation of the polar lower stratospheric temperature.

Assuming that the 22 years are independent and that the residual errors are normally distributed, the 0.82 correlation is significant at a confidence level greater than 99.9%. If we assume that there are possible errors in the calculated heat flux of up to 30% peak-to-peak [*Newman and Nash,* 2000] we can determine what effect this has on the correlation by performing a Monte Carlo simulation. We added normally distributed "noise" to the calculated heat flux with a scaling of 15% of the standard deviation of this heat flux and performed 10,000 trials. We found a mean correlation value of 0.81 with 90% confidence limits of 0.78 and 0.84 and 99% confidence limits of 0.76 and 0.86. Our correlation value of 0.82 is not statistically different from the mean of the Monte Carlo simulation so we can conclude that the errors in the heat flux observations do not significantly change the relationship we find.

We also performed exactly the same calculations using the NCEP/CPC data and found correlations of 0.85 and 0.35, respectively. These values help to confirm that the relationships we find are not based on the uniqueness within a particular data set, but upon real processes in the atmosphere.

A similar correlation between the vortex breakup date and the heat flux was found

by *Waugh et al.*, [1999]. They indicate a strong relationship between temperatures, vortex persistence (breakup date), and heat flux (calculated over the prior two months). However, they also found that the extremely low temperatures and late breakup dates in the 1990s were not reflected in extremely low heat fluxes.

The relationship of the mid-latitude lower stratospheric eddy heat flux to the entire temperature field has been determined using a 1-point correlation map. Instead of an average polar temperature, the same 22-year heat flux time series used in Figure 1 is correlated with each latitude and pressure in the March 1–15 average zonal-mean temperature fields for the 22 years of 1979 to 2000. This eddy heat flux correlation with the temperature field is shown in Plate 1a. Large positive correlations cover the entire region from about 60°N to the pole, and from the tropopause up to 20 hPa. The correlation has a maximum value greater than 0.8. We also note the strong negative correlation near the tropical tropopause ($r < -0.5$). Correlations of 0.6 and 0.5 are significant at the 99% and 98.3% confidence levels, respectively. Again, the CPC data show a similar pattern to the NCEP/NCAR reanalyses.

Plate 1

In contrast, the correlation field between the heat flux averaged over the same period as the temperatures (March 1–15) is weaker and has poorer spatial coherence (not shown).

The strong correlations exhibited in Figure 1a and Plate 1a are in good agreement with our theoretical considerations. We expect stronger wave driving of the stratosphere to enhance the Brewer-Dobson circulation. The enhanced sinking motion in the polar region will increase the temperature, while the concomitant rising motion in the

tropics will lead to lower tropical temperatures. The poorer correlations seen in the simultaneous period (Figure 1b) are also expected. The polar temperature is controlled by the accumulation of stratospheric warming wave events over the prior 20–60 days, and the slow radiative relaxation.

The heat flux time series and its interannual variation is dominated by planetary-scale waves. We can partition the total heat flux variations shown in Figure 1 and used in Plate 1a into the flux due to zonal harmonic waves 1–3 and the flux due to waves 4 and higher. Plate 1b displays the correlation of the heat flux for waves 1–3 with the March 1–15 temperature field. A comparison of Plates 1a and 1b shows that restricting the heat flux to only the planetary-scale waves leads to a slight improvement of the correlation. A weak negative correlation is found with waves 4 and higher (not shown).

We can reverse our correlations and examine the relationship between the lower stratospheric polar temperature and the heat flux patterns. From Figure 1, we know that the polar lower stratospheric temperature is strongly correlated with the heat flux. The reverse of our correlations patterns shown in Plate 1 is the correlation of the 50 hPa March 1–15 temperature 60°–90°N 22-year time series with the 22 years of zonal-mean heat flux fields. This correlation pattern with the heat flux averaged over the January 15 to February 28 period is shown for the total heat flux in Plate 2a and for Plate 2 waves 1–3 in Plate 2b. The maximum correlation of the time series is found at about 65°N and 100 hPa. A significant correlation ($r > 0.6$) extends into the troposphere down to approximately 400 hPa. The correlations are rather narrow, but coherent over deep layers. As with the correlation of the waves 1–3 heat flux with the zonal-mean

temperature field in Plate 1b, the correlation of the 60°–90°N temperature with the zonal-mean planetary waves 1–3 is also slightly improved over the total heat flux.

The maximum correlation between the heat flux and the 50 hPa March 1–15 temperature 60°–90°N time series is found close to the peak of the heat flux. The white lines superimposed on Plate 2b show the magnitude of the mean heat flux. At 100 hPa, the heat flux maximum is found at about 60°N, while the temperature-heat flux correlation has it's highest value at about 65°N. Generally, the peak of the correlation is associated with the peak of the heat flux. The slight negative correlation at 100 hPa and 35°N occurs in a region where there are weak mean heat flux values.

The 45-day period, January 15 to February 28, is arbitrarily chosen using a radiative damping time scale of 20–40 days. However, the large correlations are fairly insensitive to both the averaging period and latitude range of the heat flux. For the latitudinal averaging region of 45°–75°N, the waves 1–3 heat flux correlation with the temperature is largest for the averaging period of January 22–March 7 ($r = 0.92$). The correlation can be slightly improved by also including a wider latitudinal averaging band. Averaging from 5°–75°N for the January 22–March 7 period further improves the correlation to $r = 0.94$. All of the correlations are extremely robust if the late January and February periods are included with latitudinal bounds that at least cover the region of the peak heat flux (50° -75°N).

In addition to simple time averaging for various periods, we have also exponentially weighted the heat fluxes, consistent with the integration shown in the third term of (9). Using only the heat flux at 100 hPa for waves 1–3 in the 45°–75°N zone, we have

weighted the heat flux for damping times ranging from a few days to 100 days. The optimal damping rate is 69 days, roughly consistent with our 45-day averaging period. For a 5-day damping period, the correlation of the weighted heat flux is only 0.39, and for a 30-day damping period the correlation is 0.87. There is only marginal improvement as we increase the damping times from 30 to 69 days, with a decreasing correlation for damping times greater than 69 days.

The strong correlation of the heat flux with the temperature field maximizes at 50 hPa (see Plate 1) and decreases to insignificance at 10 hPa. The altitude at which there is a maximum correlation between the 100 hPa heat flux and the temperature is a strong function of the damping rate. This effect is illustrated in Plate 3 by correlating the heat flux averaged over a 97-day period (December 1 to March 7: Plate 3a), and over a 16-day period (February 20 to March 7: Plate 3b). Plate 3 shows that the lower stratosphere (near 100 hPa) is highly correlated for the longest averaging period, while the middle stratosphere (near 20 hPa) is highly correlated for the shorter averaging period. As was shown in (9), the correlation uses the heat flux and the damping rate at the level of interest. Since, the heat flux at 100 hPa rapidly propagates upward, the 100 hPa heat flux is an excellent surrogate for the 20 hPa heat flux. Further, polar temperatures tend to radiatively relax faster at the higher altitudes [*Kiehl and Solomon*, 1986; *Shine*, 1987; *Newman and Rosenfield*, 1997; *Mlynczak et al.*, 1999], hence, the level of maximum correlation is determined by the eddy heat flux averaging period.

Plate 3

5. Comparison between a "dynamics free" temperature and the radiatively calculated temperature

The excellent correlation between the 100 hPa heat flux and the 50 hPa polar temperature allows us to estimate the polar temperature in the absence of dynamics. We make this estimate by least-squares fitting a linear relationship of the 100 hPa heat flux to the 50 hPa polar temperature, and then calculating the intercept of this line. We can fit a straight line to Figure 1a that has a constant coefficient of 199.8 K and a slope coefficient of 0.92 K m^{-1} s. The temperature of 199.8 K would be the March 1–15 temperature of the polar region in the absence of any dynamics (i.e., if the January 15 to February 28 heat flux at 100 hPa was equal to zero).

The heat flux relationship to temperature is very robust over the entire course of the winter. Again, we have used a 55-day exponential weighting consistent with the integration shown in the third term of (9) to calculate the linear relation between the heat flux and the temperature at 80°–85°N for each day over the entire year. In this case, the correlation is greater than 0.7 for the entire period from early December to early April. Thus, the theoretical relationship between the heat flux and temperature (9) is not only applicable to early March temperatures, but is true over the entire course of the winter.

We can use the heat flux relationship to temperature to calculate the polar temperature in the absence of dynamics for the entire annual cycle. Figure 2 shows the mean annual cycle of the temperature (thick line) averaged over the 22-year

period 1979–2000 in the latitude band 80°–85°N. The white line is the temperature in the absence of dynamics, calculated by linearly fitting the heat flux to temperature relationship for each day, and then plotting this linear fit's intercept. The grey shading shows the 95% confidence interval as determined from a two-sided Student's t-distribution. While the heat flux relationship to temperature is quite poor in summer, the small values of both the heat flux and temperature lead to small uncertainties in the estimated temperature intercept. During mid-winter the "dynamics free" temperature is much colder than the mean temperature.

The "dynamics free" temperature shown in Figure 2 can be compared to a radiation model estimate of the temperature in the absence of dynamics. The temperatures were calculated by time integrating the radiative term forward with a seasonal cycle and with $\overline{w}^*$ set to zero in (1), using the GSFC radiative model [*Rosenfield et al.*, 1994]. Because radiatively determined lower stratospheric temperatures are sensitive to temperatures below the troposphere, tropospheric temperatures were specified using a time varying climatology from the surface to a specified tropopause pressure. Two cases were considered using specified tropopause pressures of 200 and 100 mb. The radiatively determined temperatures for the two cases at 80°N are also shown in Figure 2 as the upper (100 mb) and lower (200 mb) dashed lines. The "radiative equilibrium" is never reached in this model integration because of the thermal inertia and the radiative time scale. Agreement between the radiatively determined temperature (dashed lines) and the "dynamics free" temperature estimate is reasonably good in mid-winter. Large temperature discrepancies are apparent in the spring, summer, and fall. Based upon a

30- to 60-day relaxation time scale, a 10 K temperature discrepancy would be accounted for by an additional 0.15–0.3 K day^{-1} heating. Such a small error is generally within the uncertainty of the heating calculation. For example, the inclusion of NO_2 shortwave heating could account for part of this discrepancy because of high NO_2 and continuous sunlight of polar summer [*Kiehl and Solomon*, 1986]. However, the inclusion of longwave cooling by N_2O and CH_4 would lead to colder radiative temperatures.

6. Connection between the heat flux and the momentum and potential vorticity fluxes

An increase of the wave driving of the stratosphere ought to be correlated with an increase in the stratospheric momentum flux and a consequent increase in the potential vorticity (PV) flux, where the PV flux is related to the Eliassen-Palm flux divergence by $\overline{v'q'} = (a\rho_0 \cos\phi)^{-1}\nabla \cdot \mathbf{F}$ and q is the potential vorticity [*Andrews et al.*, 1987]. We test this by correlating our 22-year eddy heat flux time series with both the momentum and potential vorticity flux fields for simultaneous averaging periods. We use the same periods for the correlation, since the wave propagation time scale of a few days is short compared to our radiative damping time scale of 1–2 months. Plate 4 displays the correlation of the heat flux with the momentum flux (Plate 4a) and the potential vorticity flux (Plate 4b). Planetary waves tend to propagate upward and equatorward towards the higher index of refraction region in the tropics [*Edmon et al.*, 1980]. The 100 hPa heat flux correlation with the momentum flux is consistent with the maximum

Plate 4

correlation at slightly higher altitude (30 hPa) and slightly equatorward (45°N) as a result of this wave propagation.

As the waves propagate upward, they deposit momentum and decelerate the mean flow [*Edmon et al.*, 1980]. The PV flux is the wave forcing term on the zonal-mean momentum equation, where a strong negative PV flux acts to decelerate the zonal-mean flow. This wave momentum deposition is reflected in the high degree of correlation of the heat flux with the potential vorticity flux (Plate 4b). The PV flux is well correlated over an extensive region centered on about the 30 hPa layer.

The PV flux acts to decelerate the polar night jet stream. Via the momentum equation, we expect that a strong deceleration via the PV flux will produce a weaker jet and colder polar temperatures. Again however, we expect that the PV flux will have a time-lagged impact on the strength of the jet stream. We test this by correlating the 22-year PV flux time series for the January 15–February 28 period with the zonal-mean wind and temperature fields during March 1–15. The correlation with the wind field (Plate 5a) is excellent, with the correlation extending over a tremendous vertical depth. Plate 5 Strong wave forced decelerations at the 30 hPa level via the PV flux (i.e., large negative values of the PV flux) lead to a weakened jet stream. This weakening of the flow field is coherent from the middle stratosphere into the troposphere in the 50° 60°N region.

The correlation of the PV flux time series with the temperature fields (Plate 5b) is also excellent, with a strong negative correlation poleward and below the PV flux average region. This correlation pattern results from the residual circulation. From the TEM momentum equation, a strong PV flux induced deceleration is balanced

by a poleward meridional residual circulation flow. Via our continuity equation, this poleward flow produces a downward flow near the pole, which will act to raise the polar temperature slightly below the PV flux level. Hence, the 50 hPa polar temperature is strongly anti-correlated with the mid-latitude 30 hPa PV flux.

7. Summary

The interannual variability of March polar stratospheric temperatures is principally related to the tropospheric to lower stratospheric eddy heat flux observed in the two-month period prior to early March. The March temperature is weakly related to the temporally simultaneous eddy heat flux. This January–February eddy heat flux correlation with the early March polar stratospheric temperature is caused by the planetary waves 1–3 in the eddy heat flux. A strong planetary wave eddy heat flux in the 100–400 hPa and 45°–75°N region during January–February results in a warm March polar lower stratosphere, while a weak planetary wave eddy heat flux results in a cold March polar lower stratosphere. Correlation of the January–February 100 hPa eddy heat flux with the momentum flux shows a strong positive correlation at mid-stratospheric altitudes with the simultaneous period in January–February, and weak correlations with the phase-lagged early March momentum flux. Similarly, correlation of the January–February 100 hPa eddy heat flux with the potential vorticity flux shows a generally negative correlation at mid-stratospheric altitudes with the simultaneous period in January–February, and weak correlations with the phase-lagged early March momentum flux. Correlation of the January–February 30 hPa potential

vorticity flux shows a strong positive relationship with zonal-mean wind and a strong negative relationship with the temperature field. These results are both statistically significant, and are extremely robust to averaging periods and latitude ranges. Given the uncertainties in the heat flux estimates, the polar lower stratosphere temperature is almost completely determined by the January–February 100 hPa heat flux.

This January–February heat flux correlation with the March lower stratospheric temperature is easily understood from a simple theoretical framework based on linear thermal damping. The momentum and heat flux are directly proportional to the wave activity times the horizontal and vertical group velocities, respectively [*Edmon et al.*, 1980]. Hence, large values of the heat flux represent a strong upward flux of planetary wave activity into the stratosphere. As these planetary waves move upward into the stratosphere, they tend to be refracted towards the equator and deposit easterly momentum [*Karoly et al.*, 1982]. This process is shown in Figure 3, a schematic based on Figure 3
data. The upward propagating planetary waves are associated with the strong heat flux (Figure 3, point 1). These waves move upward and equatorward depositing their easterly momentum (Figure 3, point 2). The equatorward wave refraction is shown in Plate 4a by the strong simultaneous correlation of the heat flux with the momentum flux above and equatorward of the heat flux region. The deposition of easterly momentum is reflected in Plate 4b by the strong negative correlation over a fairly broad region. This momentum deposition is balanced by a northward residual circulation (Figure 3, point 3) which acts to decelerate the jet stream. Plate 5a illustrates this deceleration with the correlation of the potential vorticity flux with the wind. A strong wave-induced deceleration results

in a weak March jet. This wave-induced meridional residual circulation causes rising motion in the tropics, and sinking motion in the polar region (Figure 3, point 4). The polar sinking motion warms the stratosphere. Plate 5b illustrates this warming with the correlation of the potential vorticity flux with the temperature. A strong wave induced deceleration results in a warm March polar region via stronger downward motion. The warm temperatures are a result of the wave events, and are not observed simultaneously with the wave event, but *after* the wave event. In the *absence* of mid-winter waves propagating into the stratosphere, the wave forced jet deceleration is weak, resulting in a stronger March polar night jet and a colder March polar lower stratosphere.

8. Conclusions

The temperature of the polar lower stratosphere during March is key to understanding polar ozone losses. Very cold years such as 1997 have led to large chlorine-catalyzed ozone losses, while warmer years have very little ozone loss. The temperature of the early March polar lower stratosphere is principally driven by the mid-winter strength and duration of planetary waves propagating into the stratosphere. The cold polar stratospheric March periods during 1997 and 2000 were directly a result of the weak January–February wave driving of the stratosphere, while the warm polar stratospheric March periods during 1998 and 1999 were driven by the strong January–February wave driving.

The fundamental driver for the polar lower stratospheric temperature is the basic radiative state. This involves the solar angle via polar night and continuous summer

daylight, and the concentrations of basic radiative gases such as CO_2, H_2O, and ozone [*Shine,* 1987]. However, the winter temperature of the polar lower stratosphere is much warmer than would be expected from purely radiative considerations [*Fels,* 1982]. This observational-based study shows that the difference between the calculated pure radiatively driven polar temperature and actual observations is due to planetary waves 1–3 driving the polar temperature away from radiative equilibrium.

In addition to the impact of the wave driving on temperatures, the wave driving also impacts the advection of ozone via the residual circulation. Years with weak wave driving have weaker residual circulations, and therefore less poleward and downward transport of ozone. Hence, weakened wave driving has a double impact on ozone by enhancing chemical loss via the cold temperatures and by lessening the resupply of ozone into the polar region via the residual circulation. The effect of the residual circulation interannual variability on polar ozone levels has been shown by *Chipperfield and Jones* [1999]. This interannual variability of the transport is directly related to the stratospheric wave driving.

The wave driving of stratospheric temperatures may also impact the water vapor concentrations in the stratosphere. As was shown in Plate 1, the wave driving is anti-correlated with the mean tropical tropopause temperature. A weakening of the wave driving would lead to warmer tropical tropopause temperatures. One of the possible factors determining the water vapor concentration is the "freeze drying" of air entering the stratosphere at the tropical tropopause [*Dessler,* 1998 and references therein]. Predictions of weakened wave driving of the stratosphere by *Shindell et al.*

[1998] in a greenhouse climate may warm the tropical tropopause region, consequently increasing the water vapor concentration in the stratosphere. Since polar stratospheric cloud formation is dependent on the water vapor concentration, a stratospheric water vapor increase will increase the occurrence of PSCs in the polar stratosphere. This increased occurrence of PSCs will permit earlier and more extensive activation of chlorine, with consequent greater ozone loss [*Kirk-Davidoff et al.,* 1999]. Hence, from our observations we can infer that the predicted reduction of the stratospheric wave driving may increase water in the stratosphere with a consequent loss of polar ozone.

Acknowledgments. We greatly appreciate the assistance of Steve Pawson, Darryn Waugh, Alan Plumb, Mark Schoeberl, and Susan Solomon for providing extremely helpful comments and discussion on this work. Ron Nagatani of NCEP CPC has always been most helpful in acquiring CPC, MRF, and radiosonde data. We also wish to thank Don Hooper of NOAA-CIRES Climate Diagnostics Center (CDC) for his help in obtaining the NCEP/NCAR analyses. Portions of the NCEP/NCAR reanalysis were provided by CDC, from their Web site at http://www.cdc.noaa.gov/. This work was carried out under the NASA Atmospheric Chemistry, Modeling, and Analysis Program.

References

Anderson, J. G., W. H. Brune, S. A. Lloyd, D. W. Toohey, S. P. Sander, W. L. Starr, M. Loewenstein, and J. R. Podolske, Kinetics of O_3 destruction by ClO and BrO within the Antarctic vortex: An analysis based on in situ ER-2 data, *J. Geophys. Res., 94*,

11,480–11,520, 1989.

Andrews, D. G., J. R. Holton, and C. B. Leovy, *Middle Atmosphere Dynamics*, Academic Press, Florida, 489 pp., 1987.

Brewer, A. W., Evidence for a world circulation provided by the measurements of helium and water vapor distribution in the stratosphere, *Quart. J. Roy. Met. Soc., 75,* 351–363, 1949.

Chipperfield M. P., and R. L. Jones, Relative influences of atmospheric chemistry and transport on Arctic ozone trends, *Nature, 400,* 551–554, 1999.

Coy L., E. R. Nash, and P. A. Newman, Meteorology of the polar vortex: Spring 1997, *Geophys. Res. Lett., 24,* 2693–2696, 1997

Dessler, A. E., A reexamination of the "stratospheric fountain" hypothesis, *Geophys. Res. Lett., 25,* 4165–4168, 1998.

Dobson, G. M. B., Origin and distribution of polyatomic molecules in the atmosphere, *Proc. Roy. Soc. London, Series A, 236,* 187–193, 1956.

Dunkerton, T., On the mean meridional mass motions of the stratosphere and mesosphere, *J. Atmos. Sci., 35,* 2325–2333, 1978.

Edmon, H. J., B. J. Hoskins, and M. E. McIntyre, Eliassen-Palm cross-sections for the troposphere, *J. Atmos. Sci., 37,* 2600–2616, 1980.

Farman, J. C., R. J. Murgatroyd, A. M. Silnickas, and B. A. Thrush, Ozone photochemistry in the Antarctic stratosphere in summer, *Quart. J. R. Met. Soc., 111,* 1013–1028, 1985.

Fels, S. B., A parameterization of scale-dependent radiative damping rates in the middle atmosphere, *J. Atmos. Sci, 39,* 1141–1152, 1982.

Finger, F. G., M. E. Gelman, J. D. Wild, M. L. Chanin, A. Hauchecorne, and A. J. Miller, Evaluation of NMC upper-stratospheric temperature analyses using rocketsonde and lidar

data, *Bull. Am. Meteorol. Soc., 74,* 789–799, 1993

Fioletov, V. E., J. B. Kerr, D. I. Wardle, J. Davies, E. W. Hare, C. T. McElroy, and D. W. Tarasick, Long-term ozone decline over the Canadian Arctic to early 1997 from ground-based and balloon observations, *Geophys. Res. Lett., 24,* 2705–2708, 1997.

Fusco, A. C., and M. L. Salby, Interannual variations of total ozone and their relationship to variations of planetary wave activity, *J. Climate, 12,* 1619–1629, 1999.

Gelman, M. E., A. J. Miller, K. W. Johnson, and R. M. Nagatani, Detection of long-term trends in global stratospheric temperature from NMC analyses derived from NOAA satellite data, *Adv. Space Res., 6*(10), 17–26, 1986.

Haynes, P. H., C. J. Marks, M. E. McIntyre, T. G. Shepherd, and K. P. Shine, On the "downward control" of extratropical diabatic circulations by eddy-induced mean zonal forces, *J. Atmos. Sci., 48,* 651–678, 1991.

Kalnay, E., M. Kanamitsu, R. Kistler, W. Collins, D. Deaven, L. Gandin, M. Iredell, S. Saha, G. White, J. Woollen, Y. Zhu, M. Chelliah, W. Ebisuzaki, W. Higgins, J. Janowiak, K. C. Mo, C. Ropelewski, J. Wang, A. Leetmaa, R. Reynolds, R. Jenne, and D. Joseph, The NCEP/NCAR 40-year reanalysis project, *Bull. Am. Meteorol. Soc., 77,* 437–471, 1996.

Kiehl, J. T., and S. Solomon, On the radiative balance of the stratosphere, *J. Geophys. Res., 43,* 1525–1534, 1986.

Kirk-Davidoff, D. B., E. J. Hintsa, J. G. Anderson, and D. W. Keith, The effect of climate change on ozone depletion through changes in stratospheric water vapor, *Nature, 402,* 399–401, 1999.

Karoly, D. J., and B. J. Hoskins, Three dimensional propagation of planetary-waves, *J. Met. Soc. of Japan, 60,* 109–123, 1982.

London, J., Ozone variations and their relation to stratospheric warmings. Symposium on Stratospheric and Mesospheric Circulation, Vol. 36, Meteorologische Abhandlungen der Freien Universitt Berlin, 299–310, 1963.

Mlynczak, M. G., C. J. Mertens, R. R. Garcia, and R. W. Portmann, A detailed evaluation of the stratospheric heat budget, 2. Global radiation balance and diabatic circulations, *J. Geophys. Res., 104,* 6039–6066, 1999.

Nagatani, R. M., A. J. Miller, K. W. Johnson, and M. E. Gelman, An eight-year climatology of meteorological and SBUV ozone data, NOAA Tech. Rep. NWS 40, Natl. Weather Serv., Washington, D. C., 125 pp., 1988.

Newman P. A., and E. R. Nash, Quantifying the wave driving of the stratosphere, *J. Geophys. Res., 105,* 12,485–12,497, 2000.

Newman P. A., and J. E. Rosenfield, Stratospheric thermal damping times, *Geophys. Res. Lett., 24,* 433–436, 1997.

Newman P. A., L. R. Lait, and M. R. Schoeberl, The morphology and meteorology of southern hemisphere spring total ozone mini-holes, *Geophys. Res. Lett., 15,* 923–926, 1988.

Newman, P. A., J. F. Gleason, R. D. McPeters, and R. S. Stolarski, Anomalously low ozone over the Arctic, *Geophys. Res. Lett., 24,* 2689–2692, 1997.

Pawson, S., and M. Fiorino, A comparison of reanalyses in the tropical stratosphere. Part 1: thermal structure and the annual cycle, *Clim. Dyn., 24,* 631–644, 1998.

Pawson, S., and B. Naujokat, Trends in daily wintertime temperatures in the northern stratosphere, *Geophys. Res. Lett., 14,* 575–578, 1997.

Pawson, S., and B. Naujokat, The cold winters of the middle 1990s in the northern lower stratosphere, *J. Geophys. Res., 104,* 14,209–14,222, 1999.

Plumb, R. A., Eddy fluxes of conserved quantities by small-amplitude waves, *J. Atmos. Sci., 36,* 1699–1704, 1979.

Poole, L. R., and M. C. Pitts, Polar stratospheric cloud climatology based on Stratospheric Aerosol Measurement II observations from 1978 to 1989, *J. Geophys. Res., 99,* 13,083–13,089, 1994.

Randel, W. J., The evaluation of winds from geopotential height data in the stratosphere, *J. Atmos. Sci., 44,* 3097–3120, 1987.

Rosenfield, J. E., P. A. Newman, and M. R. Schoeberl, Computations of diabatic descent in the stratospheric polar vortex, *J. Geophys. Res., 99,* 20,713–20,723, 1994.

Santer, B. D., J. J. Hnilo, T. M. L. Wigley, J. S. Boyle, C. Doutriaux, M. Fiorino, D. E. Parker, and K. E. Taylor, Uncertainties in observationally based estimates of temperature change in the free atmosphere, *J. Geophys. Res., 104,* 6305–6333, 1999.

Shindell, D. T., D. Rind, and P. Lonergan, Increased polar stratospheric ozone losses and delayed eventual recovery owing to increasing greenhouse-gas concentrations, *Nature, 392,* 589–592, 1998.

Shine, K. P., The middle atmosphere in the absence of dynamic heat fluxes, *Q. J. Roy. Met. Soc., 113,* 603-633, 1987.

Waugh, D. W., W. J. Randel, S. Pawson, P. A. Newman, and E. R. Nash, Persistence of the lower stratospheric polar vortices, *J. Geophys. Res., 104,* 27,191–27,201, 1999.

Zurek, R. W., G. L. Manney, A. J. Miller, M. E. Gelman, and R. M. Nagatani, Interannual variability of the north polar vortex in the lower stratosphere during the UARS mission, *Geophys. Res. Lett., 23,* 289–292, 1996.

Received _____

Figure 1. Temperature (50 hPa, March 1–15, and 60°–90°N) plotted against the total heat flux, $\overline{v'T'}$, (100 hPa and 45°–75°N) for (a) January 15 to February 28 and (b) March 1–15. The individual years are as indicated.

Plate 1. Correlation of the 22 years (1979–2000) of the a) total and b) waves 1–3 components of heat flux (100 hPa, January 15 to February 28, and 45°–75°N) with the temperature fields (March 1–15). Superimposed is the tropopause (thick purple line) as determined from the Brunt-Vaisalla frequency and a) the zonal-mean zonal wind and b) the 22-year average of the heat flux from waves 1–3 (white lines).

Plate 2. As in Figure 2 but for the correlation of temperature (50 hPa, 60°–90°N, and March 1–15) with the a) total and b) waves 1–3 components of heat flux fields (100 hPa and January 15 to February 28).

Plate 3. Correlation of the 22 years (1979–2000) of the heat flux (waves 1–3, 100 hPa, 50°–80°N) averaged over a) December 1 to March 7 and b) February 20 to March 7 with the temperature fields (March 1–15). Superimposed is the tropopause (thick purple line) as determined from the Brunt-Vaisalla frequency and the 22-year average of the heat flux from waves 1–3 (white lines).

Plate 4. Correlation of the 22 years (1979–2000) of the heat flux (100 hPa and 45°–75°N) with a) the momentum flux and b) the potential vorticity flux fields. All quantities are from January 15 to February 28, waves 1–3. Superimposed is the tropopause (thick purple line) as determined from the Brunt-Vaisalla frequency and the zonal-mean zonal wind (white lines).

Figure 2. Temperature (50 hPa and 80°–85°N) averaged for the 22-year period 1979–2000 (thick solid line) and calculated radiatively using ozone, water, and CO_2 (dashed line). The white line shows the estimated "dynamics free" temperature using the heat flux relationship to temperature. The grey shading shows the 95% confidence limits on the "dynamics free" temperature estimates.

Figure 3. Schematic illustration of planetary waves propagating into the stratosphere (1), slowly bending towards the equator (2), depositing easterly momentum (3), and inducing a residual circulation that causes uplift in the tropics and sinking in the polar region (4). The short arrows illustrate the wave propagation while the thick line with arrows shows the residual circulation. The thin solid lines show the wind speed, the dotted line shows the tropopause, and the dashed lines show the potential vorticity flux or wave-driven wind deceleration.

Plate 5. As in Figure 4 but for the correlation of the potential vorticity flux (30 hPa, 45°–75°N, January 15 to February 28, and waves 1–3) with the March 1–15 a) zonal-mean wind and b) temperature fields.

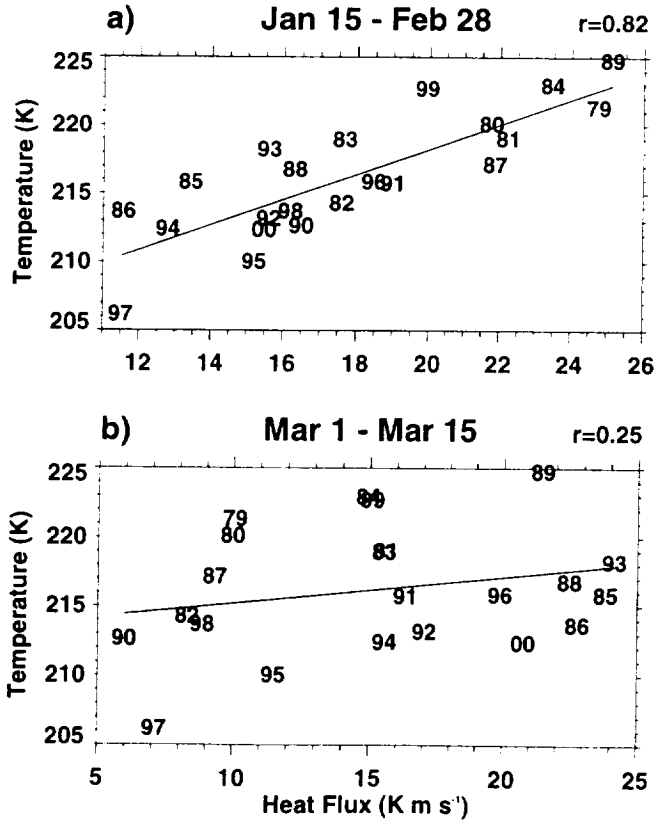
a)
Jan 15 - Feb 28
r=0.82
Temperature (K)
225
220
215
210
205
12
14
16
18
20
22
24
26
89
99
84
79
80
81
83
93
88
87
85
96
91
86
94
82
98
00
90
95
97
b)
Mar 1 - Mar 15
r=0.25
Temperature (K)
225
220
215
210
205
5
10
15
20
25
Heat Flux (K m s⁻¹)
89
79
80
87
93
88
85
91
96
82
98
90
94
92
00
86
95
97

P1

B

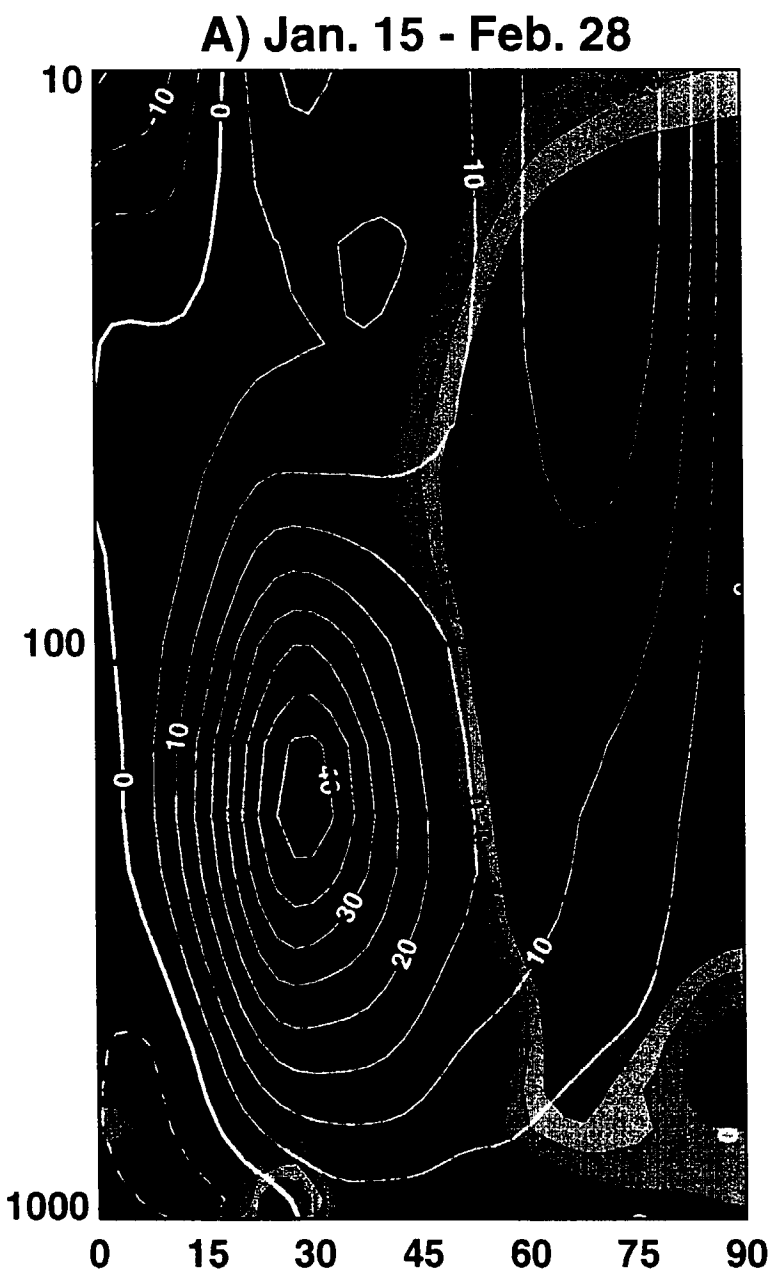
A) Jan. 15 - Feb. 28
10
100
1000
0
15
30
45
60
75
90
-10
0
10
20
30
40

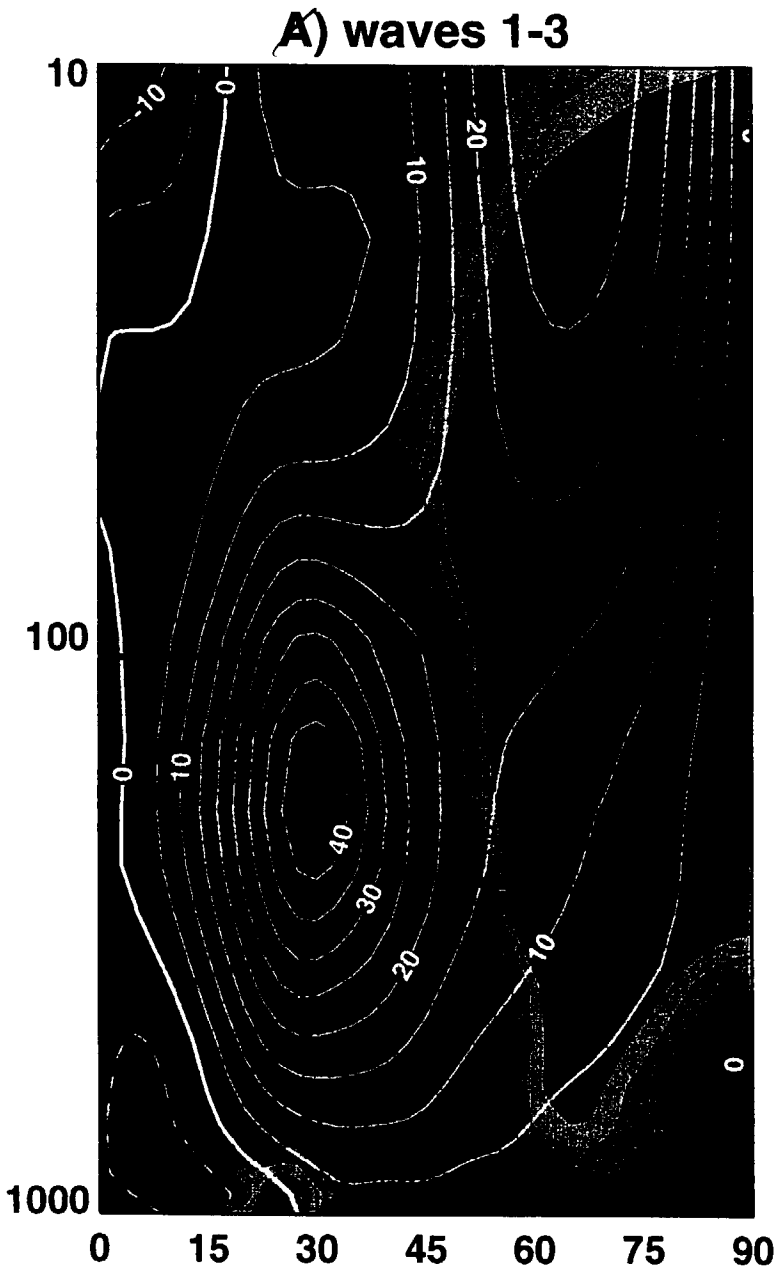
A) waves 1-3
10
100
1000
0
15
30
45
60
75
90
-10
0
10
20
30
40

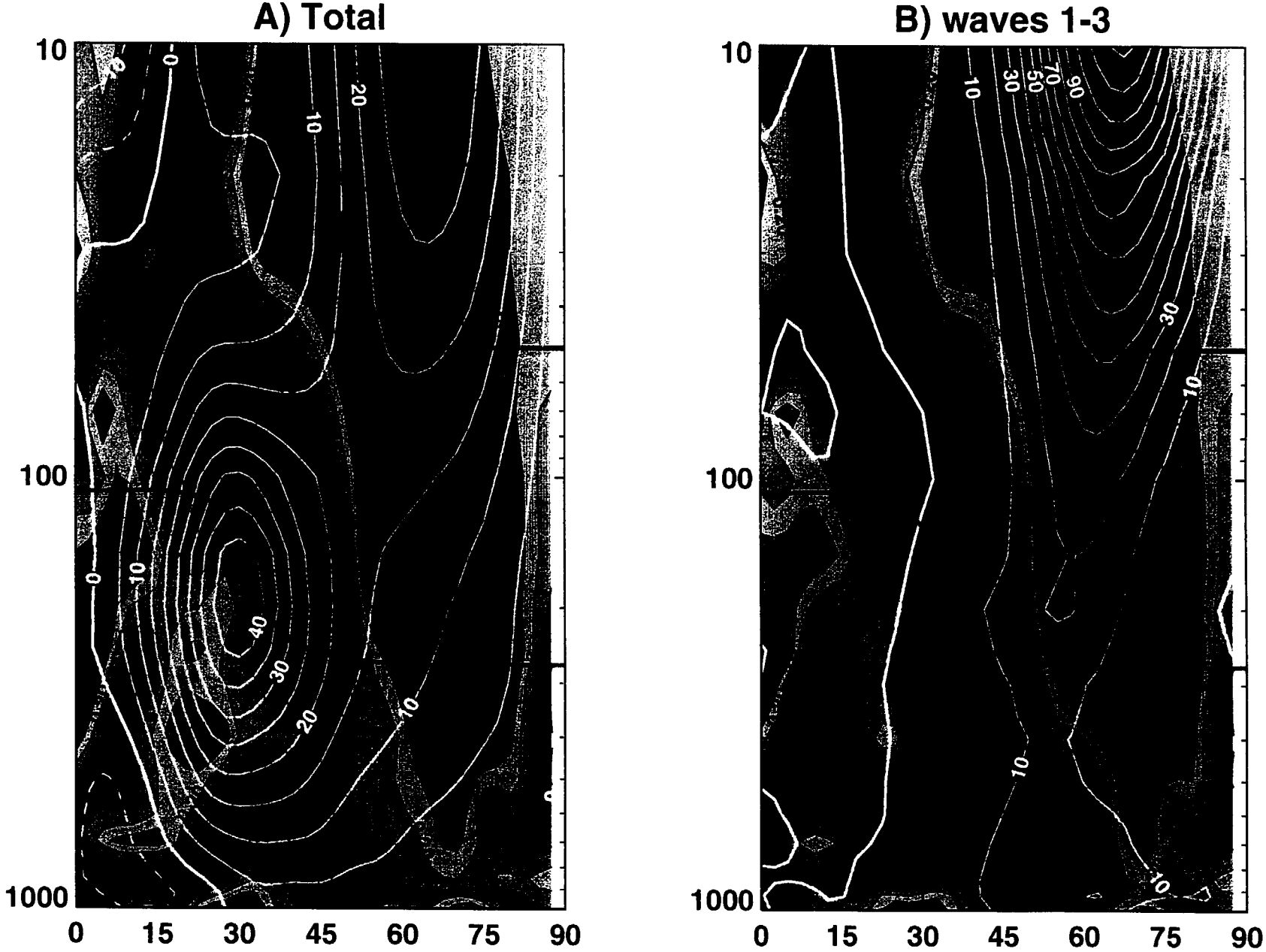
A) Total
B) waves 1-3
10
100
1000
0
15
30
45
60
75
90

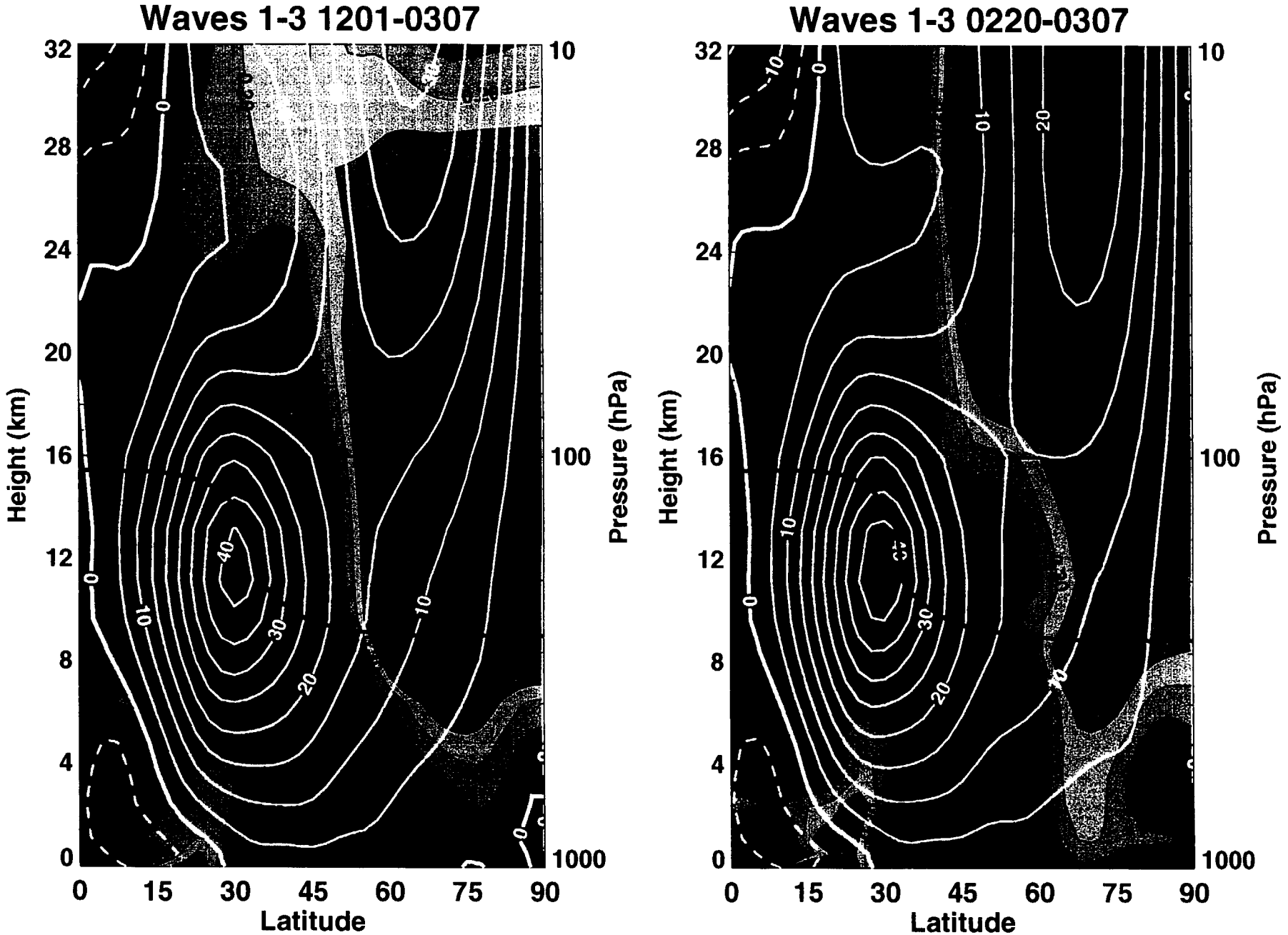
Waves 1-3 1201-0307
Waves 1-3 0220-0307
Height (km)
Pressure (hPa)
Latitude
0
4
8
12
16
20
24
28
32
10
100
1000
0
15
30
45
60
75
90

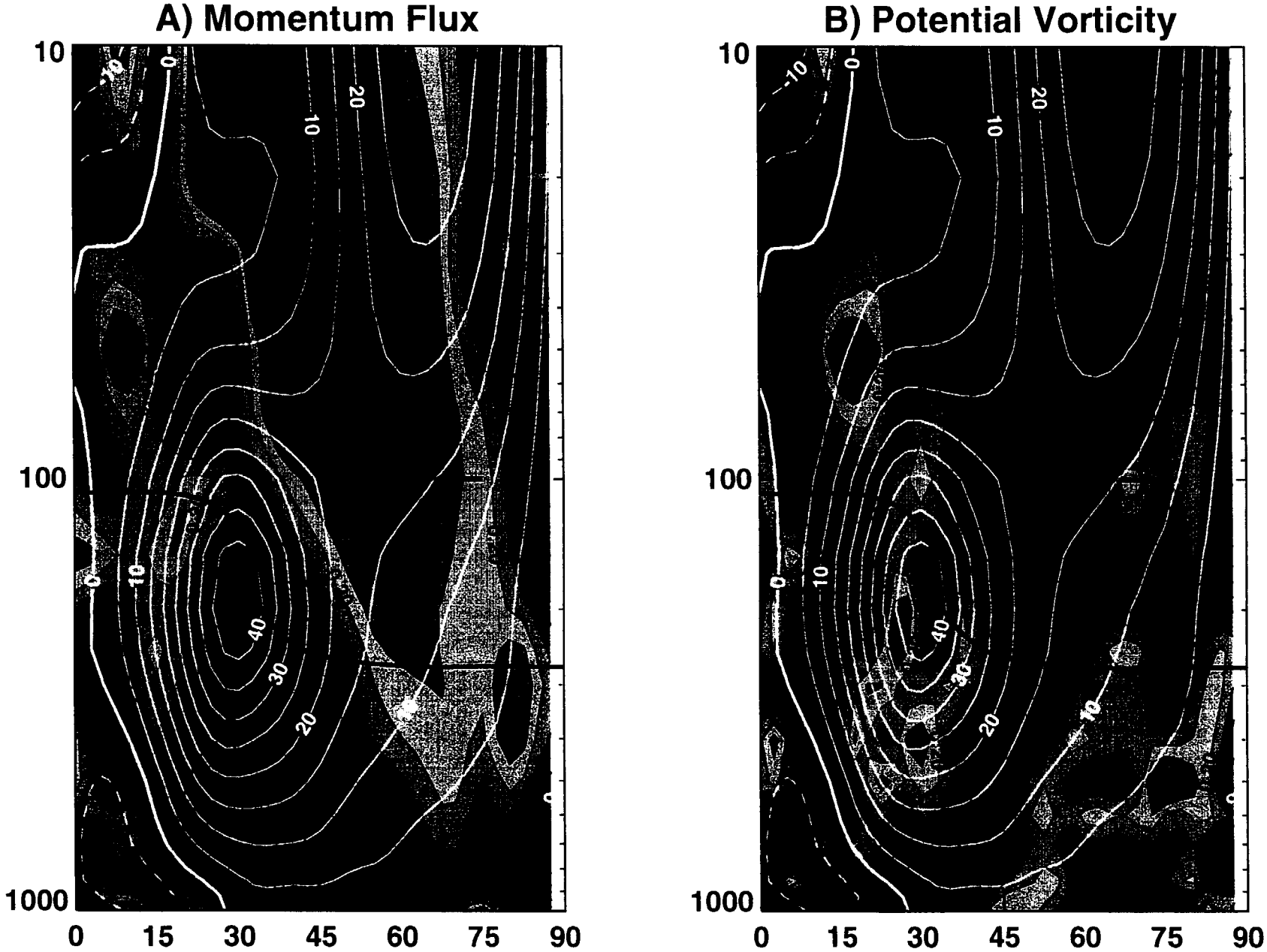
A) Momentum Flux
B) Potential Vorticity
10
100
1000
0
15
30
45
60
75
90

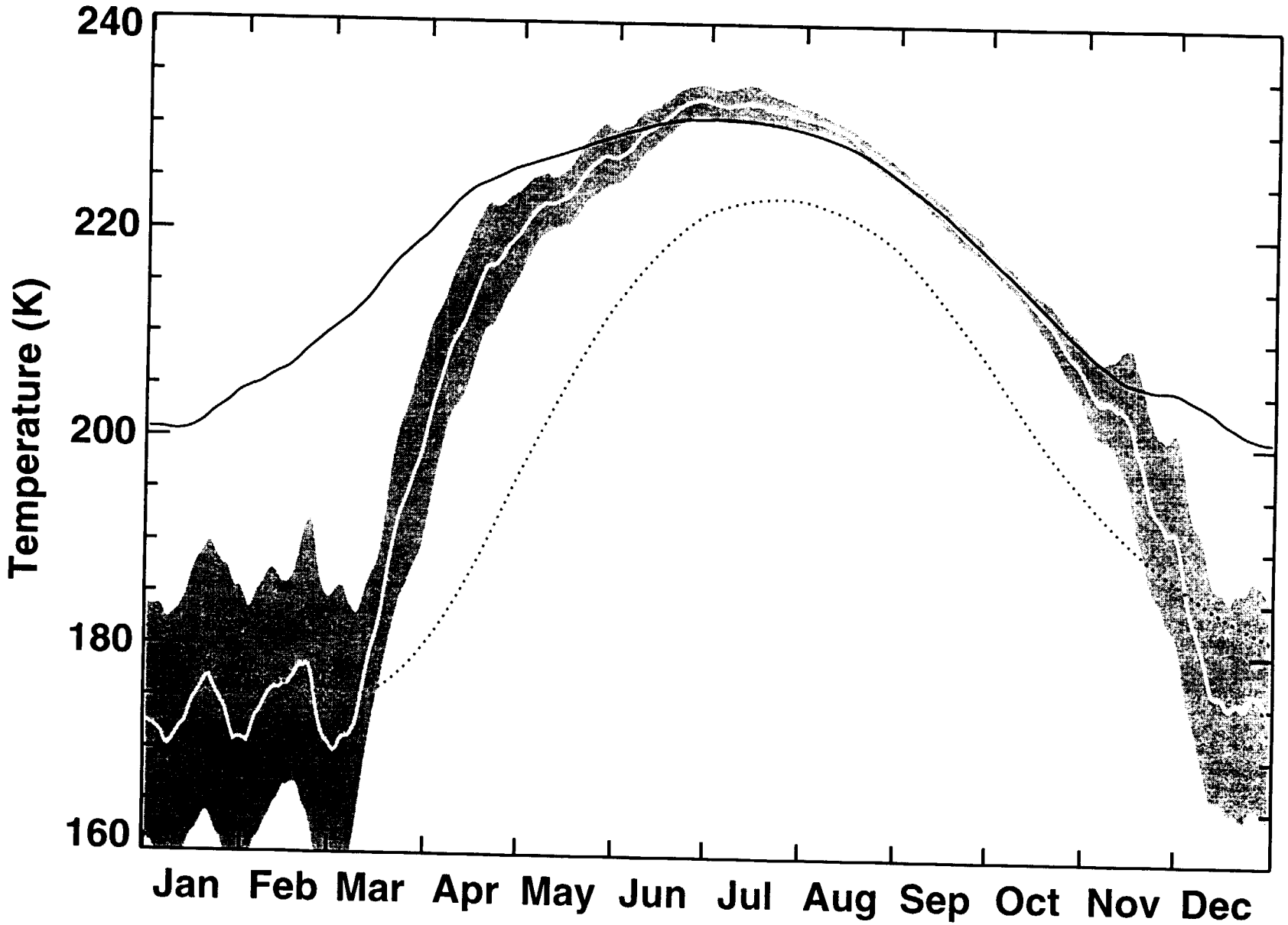
240
220
200
180
160
Temperature (K)
Jan
Feb
Mar
Apr
May
Jun
Jul
Aug
Sep
Oct
Nov
Dec

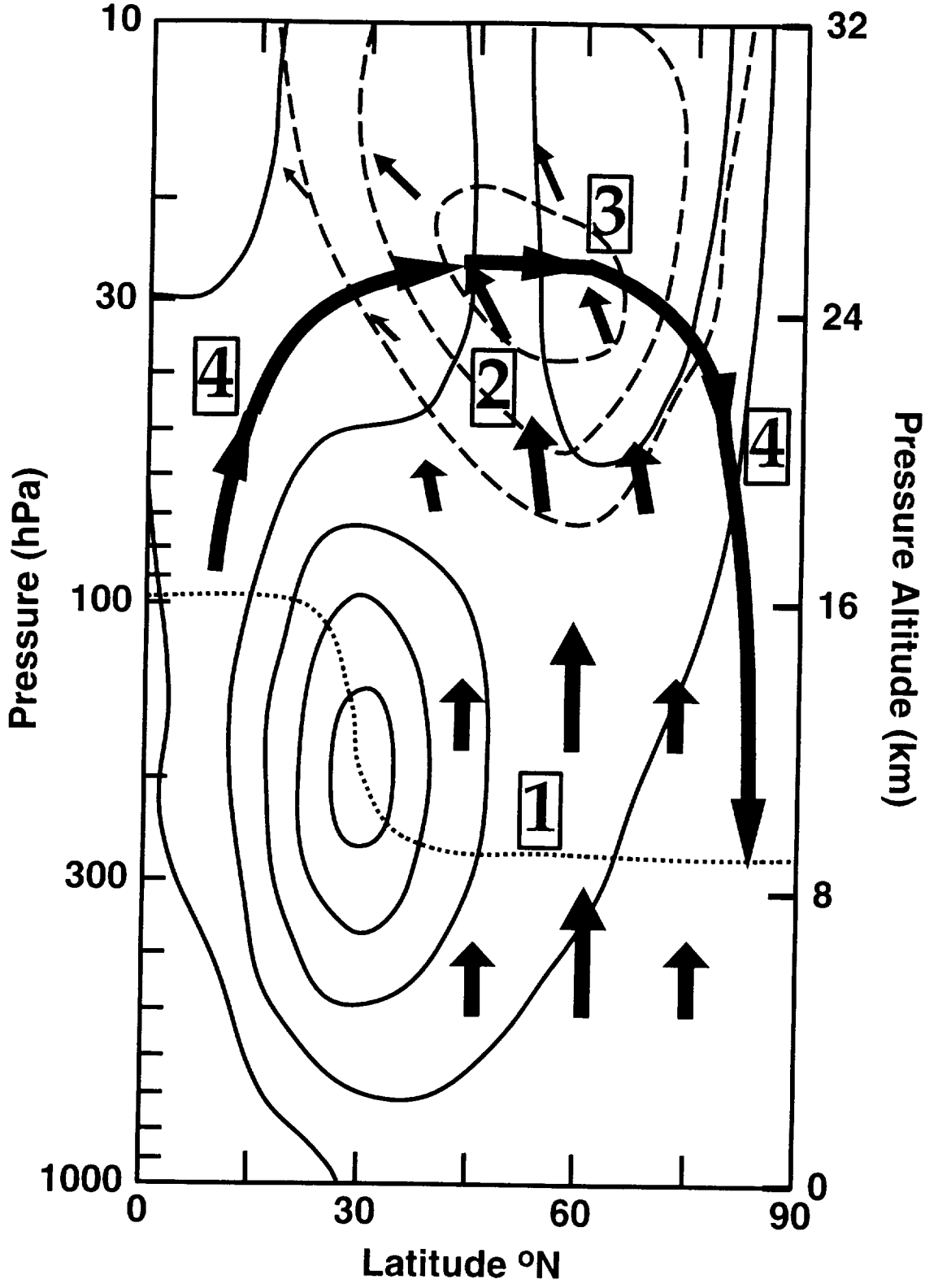
10
30
100
300
1000
Pressure (hPa)
32
24
16
8
0
Pressure Altitude (km)
0
30
60
90
Latitude °N
1
2
3
4
4

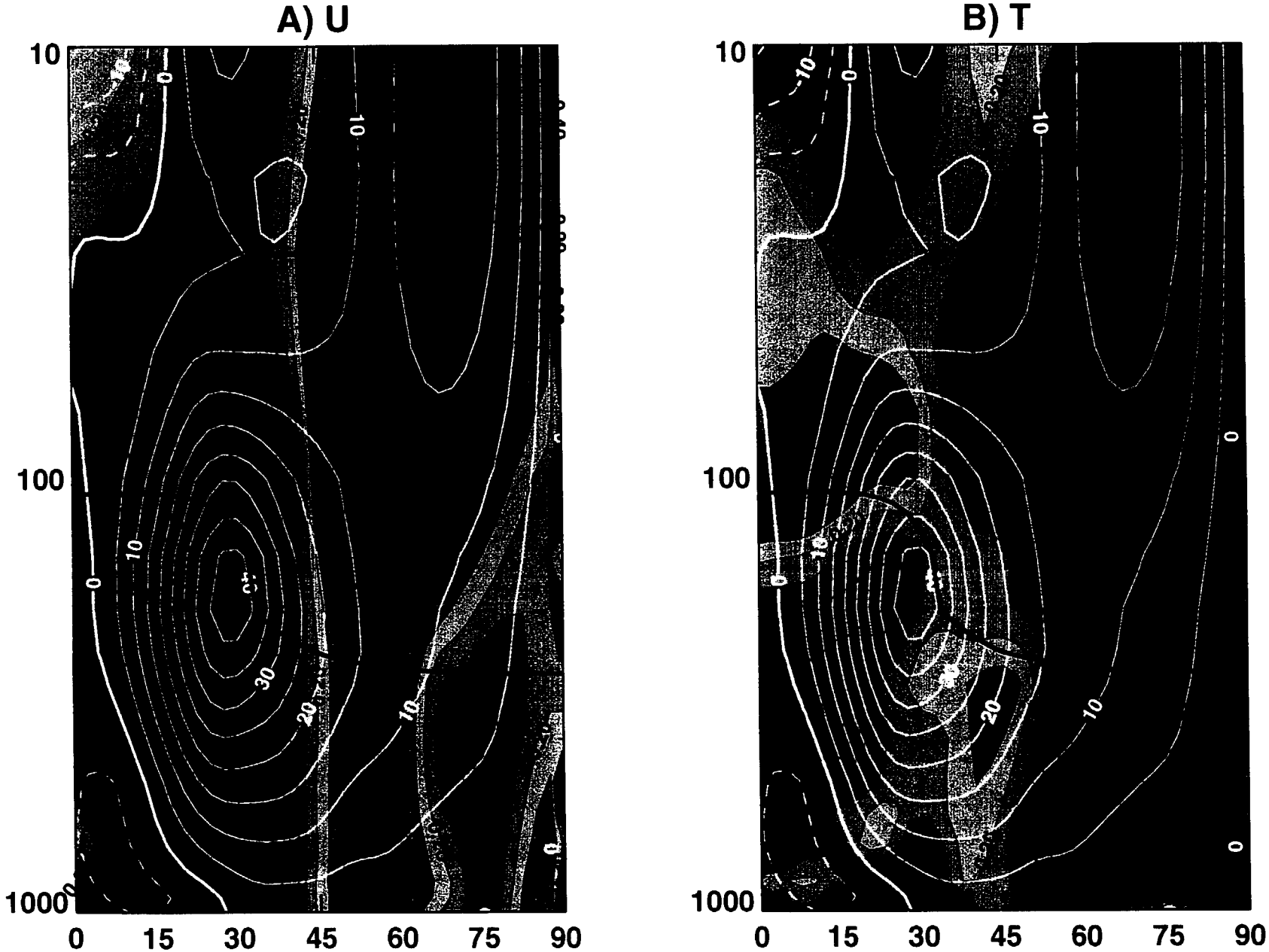
A) U
B) T
10
100
1000
0
15
30
45
60
75
90